Additional microstructure-graded examples

1 Microstructure-graded simply-supported beam

The simply supported beam analysis employs symmetry about the midpoint to model only the left half, reducing computational complexity. The modeled section has a length of 50 mm, height of 10 mm, and thickness of 1 mm. A uniformly distributed downward load of 100 N is applied at the right end, representing half of the full beam configuration. Boundary conditions enforce zero vertical displacement at the left end and zero horizontal displacement at the right end, creating mirror symmetry consistent with a full 100 mm beam under 200 N center point load. The mesh utilizes Delaunay triangulation with 500×100 nodes along length and height, as shown in Fig. 1 (a).

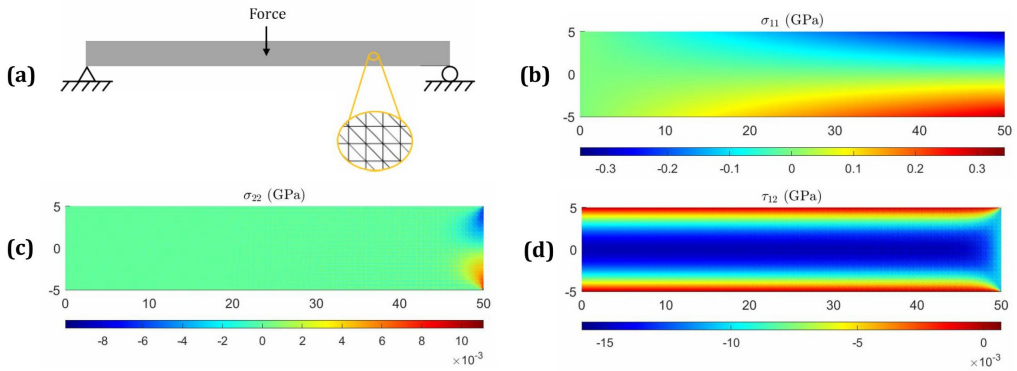

Figure 1: (a) Schematic diagram of the analyzed simply supported beam subjected to a mid-span load, along with the mesh discretization; and corresponding stress component distributions over the left half of the beam at the initial iteration: (b) σ_{11}, (c) σ_{22}, and (d) τ_{12}. Dimensions are in 'mm', and stresses are in 'GPa'.

Initial isotropic properties yield stress distributions in Fig. 1 (b-d). The axial stress component σ_{11} emerges as the primary strain energy contributor, varying from zero at the left end to maximum at the center, corresponding to the bending moment distribution. The shear stress τ_{12} remains approximately constant along the length but decreases with distance from the neutral axis; however, its magnitude insufficiently influences the strain energy function. Consequently, only σ_{11} variation directly drives the optimized stiffness distribution in Fig. 2. This distribution pattern resembles the cantilever beam case but reversed due to opposite bending moment orientation. The optimized C_{11} exhibits a minimum near the beam's midline where σ_{11} is zero. Meanwhile, relatively higher τ_{12} values near the neutral axis elevate optimal C_{12} and C_{66} in that region. This produces a tapered, cone-shaped stiffness distribution with the cone oriented oppositely to the cantilever case. The cone thickness diminishes progressively with increasing bending moment along beam length, reflecting localized material property adaptation to the evolving stress environment.

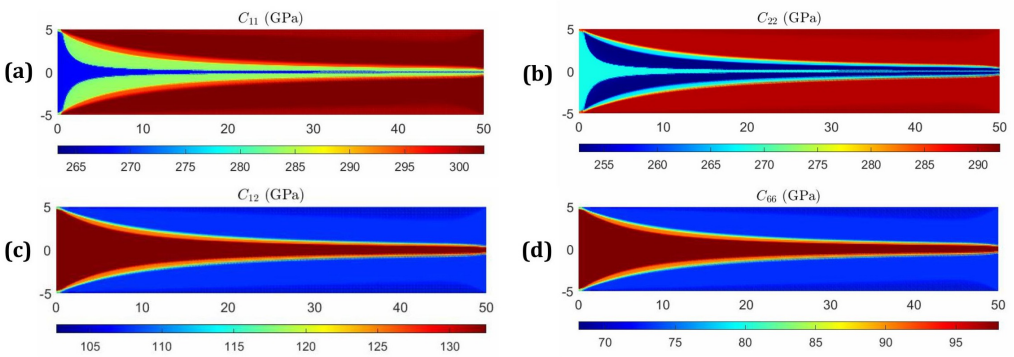

Figure 2: Finalized distributions of optimal properties across left half of the simply supported beam under the conditions shown in Fig. 1 after the 4^{th} iteration: (a) C_{11}, (b) C_{22}, (c) C_{12}, and (d) C_{66}. Dimensions are in 'mm', and stiffness coefficients are in 'GPa'.

2 Microstructure-graded L-shaped frame

The L-shaped thin frame consists of horizontal and vertical segments, each 60 mm long with 10 mm in-plane thickness and 1 mm out-of-plane thickness. A downward distributed load of 50 N is applied uniformly across the right edge of the horizontal segment, as illustrated in Fig. 3 (a). The horizontal arm behaves as a cantilever beam while the vertical segment functions as a supporting column under combined bending and axial compression. Both horizontal and vertical displacements are fully restrained at the bottom face of the vertical segment, effectively clamping the structure. The mesh employs a 301×301 structured grid followed by Delaunay triangulation, with elements in the pocket region excluded through centroid filtering for computational efficiency.

The three in-plane stress components from initial property allocation appear in Fig. 3 (b-d). The diverse stress magnitudes across all components significantly influence the optimal stiffness distribution shown in Fig. 4. The normal stress σ_{11} exhibits greater variability in the horizontal segment due to bending-induced fluctuations, while remaining relatively uniform throughout the vertical segment. Conversely, σ_{22} demonstrates more pronounced variation in the vertical segment with near-constant values in the horizontal portion. This pattern emerges from applied loading that induces bending moments in both segments: σ_{11} primarily governs the horizontal portion while σ_{22} dominates the vertical portion. Additionally, the vertical segment experiences consistent axial compressive stress distributed evenly across its elements. The optimized stiffness field reveals dominant C_{11} values in the horizontal segment and higher C_{22} values in the vertical segment, as shown in Fig. 4 (a,b), corresponding to respective normal stress concentration directions. The shear stress component τ_{12} is substantially elevated near the L-frame junction where the load path changes direction, causing significant stress redistribution. This localized shear concentration results from force transfer between orthogonal members, leading to elevated optimized values of shear-related stiffness coefficients C_{12} and C_{66} in this transitional zone. This shear response extends along the neutral axis of the horizontal segment where shear stresses remain relatively high, clearly reflected in the optimized stiffness distributions of Fig. 4 (c,d), highlighting shear stress behavior influence on anisotropic material property design in structurally critical regions.

3 Performance improvement

The performance improvement trend of the microstructure-graded simply supported beam and L-shaped frame (as shown in Fig. 5) remains consistent with the observations previously noted under both in-plane and out-of-plane loading scenarios.

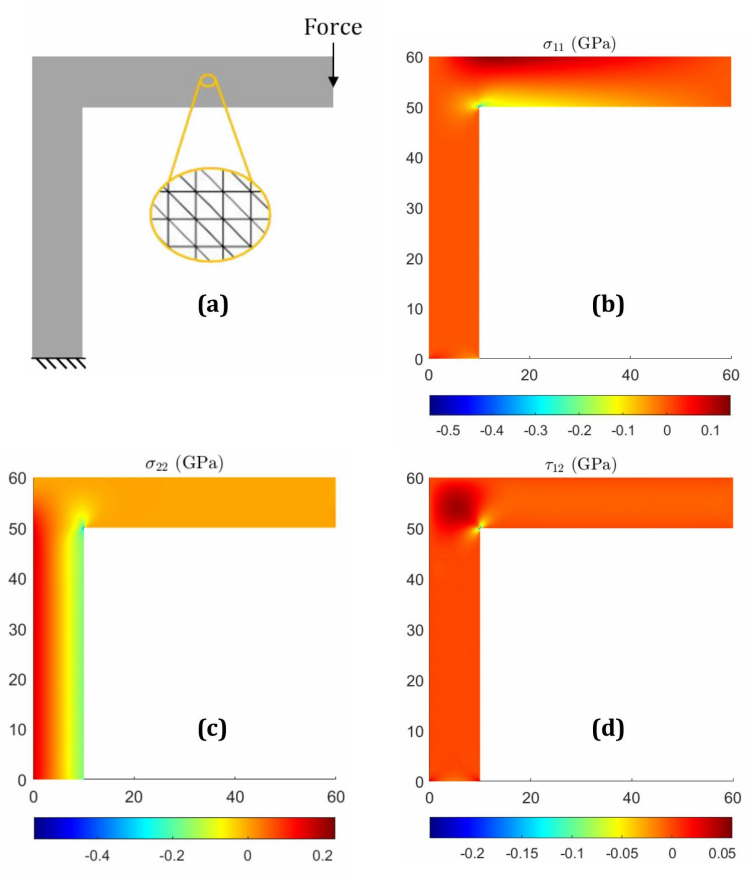

Figure 3: (a) Schematic diagram of the L-shaped frame subjected to an end load, along with the mesh discretization; and corresponding stress component distributions over the frame at the initial iteration: (b) σ_{11}, (c) σ_{22}, and (d) τ_{12}. Dimensions are in 'mm', and stresses are in 'GPa'.

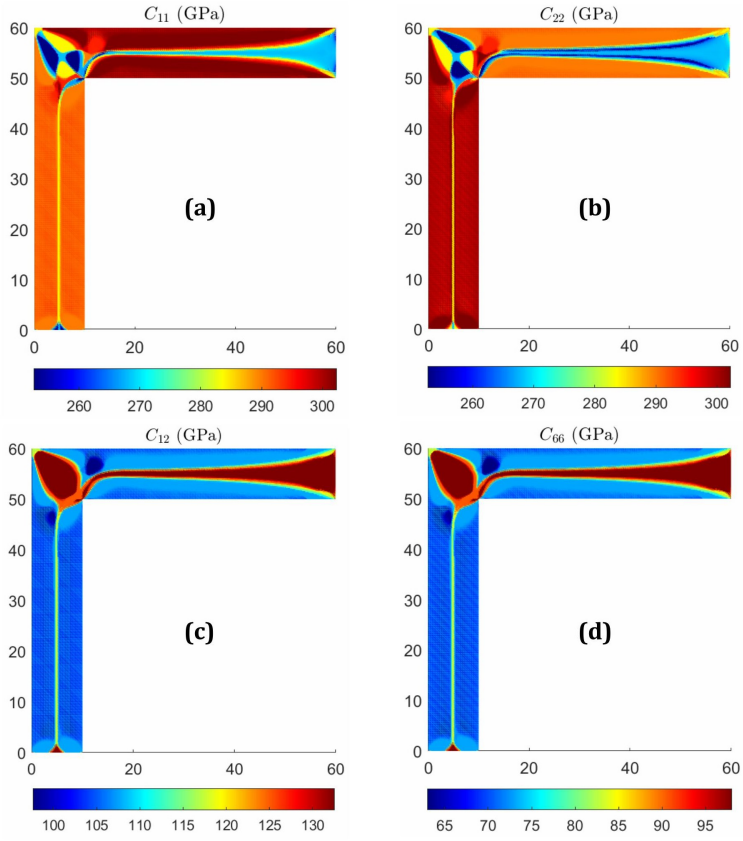

Figure 4: Finalized distributions of optimal properties across the L-shaped frame under the conditions shown in Fig. 3 after the 4^{th} iteration: (a) C_{11}, (b) C_{22}, (c) C_{12}, and (d) C_{66}. Dimensions are in 'mm', and stiffness coefficients are in 'GPa'.

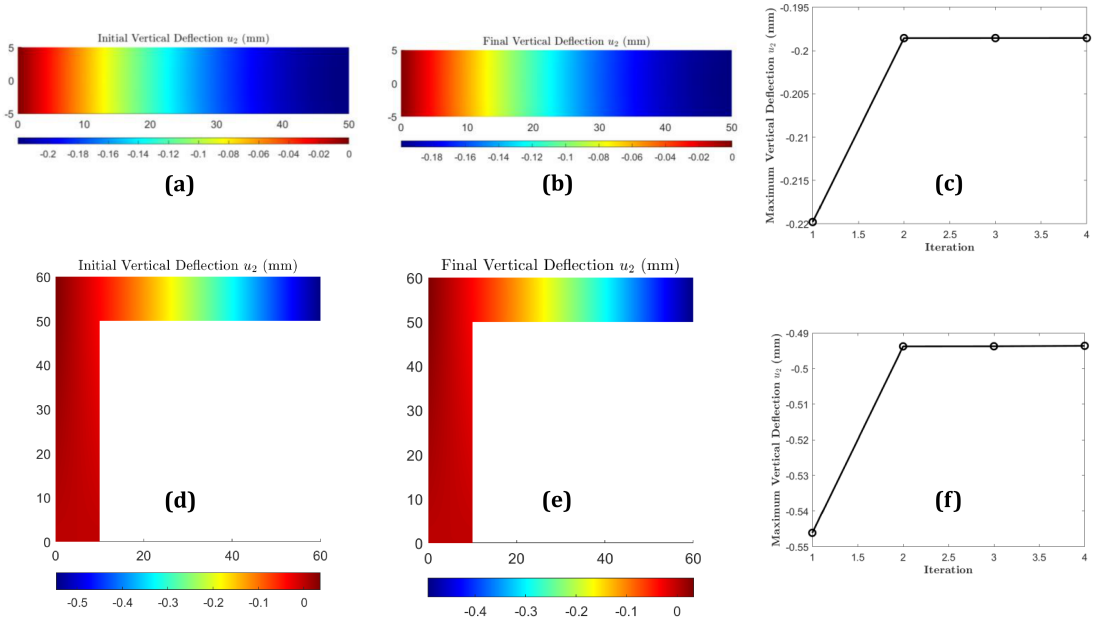

Figure 5: Comparative vertical deflection analysis of in-plane loaded structures:(a)–(c) simply supported beam with mid load (left half); (d)–(f) L-shaped frame with end load. (a) and (d) reference structures with uniform isotropic properties; (b) and (e) show the optimized structures with functionally graded orthotropic properties; (c) and (f) demonstrate deflection versus optimization iterations.